Bioorganic & Medicinal Chemistry 24 (2016) 4008–4015

Contents lists available at ScienceDirect

Bioorganic & Medicinal Chemistry

journal homepage: www.elsevier.com/locate/bmc

Kinetic and structural insights into the binding of histone deacetylase 1 and 2 (HDAC1, 2) inhibitors

Florence F. Wagner [a,*], Michel Weïwer [a], Stefan Steinbacher [b], Adrian Schomburg [b], Peter Reinemer [b], Jennifer P. Gale [a], Arthur J. Campbell [a], Stewart L. Fisher [c], Wen-Ning Zhao [d], Surya A. Reis [d], Krista M. Hennig [d], Méryl Thomas [a], Peter Müller [e], Martin R. Jefson [f], Daniel M. Fass [d], Stephen J. Haggarty [d], Yan-Ling Zhang [a], Edward B. Holson [a,*,†]

[a] Stanley Center for Psychiatric Research, Broad Institute of MIT and Harvard, 75 Ames Street, Cambridge, MA, USA
[b] Proteros Biostructures GmbH, Bunsenstr. 7a, 82152 Martinsried, Germany
[c] SL Fisher Consulting, LLC, 18 Harrington Road, Framingham, MA, USA
[d] Chemical Neurobiology Laboratory, Center for Human Genetic Research, Massachusetts General Hospital, Department of Neurology and Psychiatry, Harvard Medical School, Boston, MA, USA
[e] X-ray Diffraction Facility, MIT Department of Chemistry, 77 Massachusetts Avenue, 2-325, Cambridge, MA, USA
[f] Rodin Therapeutics Inc., 400 Technology Square, 10th Floor, Cambridge, MA, USA

ARTICLE INFO

Article history:
Received 24 May 2016
Revised 17 June 2016
Accepted 18 June 2016
Available online 22 June 2016

Keywords:
HDAC inhibitors
Isoform selectivity
Kinetic selectivity
Target engagement
Acetylation

ABSTRACT

The structure–activity and structure–*kinetic* relationships of a series of novel and selective *ortho*-aminoanilide inhibitors of histone deacetylases (HDACs) 1 and 2 are described. Different kinetic and thermodynamic selectivity profiles were obtained by varying the moiety occupying an 11 Å channel leading to the Zn^{2+} catalytic pocket of HDACs 1 and 2, two paralogs with a high degree of structural similarity. The design of these novel inhibitors was informed by two ligand-bound crystal structures of truncated *h*HDAC2. **BRD4884** and **BRD7232** possess kinetic selectivity for HDAC1 versus HDAC2. We demonstrate that the binding kinetics of HDAC inhibitors can be tuned for individual isoforms in order to modulate target residence time while retaining functional activity and increased histone H4K12 and H3K9 acetylation in primary mouse neuronal cell culture assays. These chromatin modifiers, with tuned binding kinetic profiles, can be used to define the relation between target engagement requirements and the pharmacodynamic response of HDACs in different disease applications.

1. Introduction

Imbalance in the status of chromatin post-translational modifications, such as histone acetylation and methylation, plays a significant role in many human diseases as it tightly controls and alters chromatin architecture regulating gene transcription.[1] The role of epigenetic modifications is well known in cancer,[2] and increasing evidence supports contributions in non-oncology indications such as diabetes,[3] infectious disease (HIV),[4] or neurodegenerative and psychiatric disorders.[5] In the latter case, there is mounting evidence implicating dysfunction in acetylation status, a chromatin modification mediated by histone acetyltransferases (HATs) and histone deacetylases (HDACs). Understanding the role of the individual HDAC isoforms and development of highly potent and selective inhibitors of each isozyme has increased in the past decade.[6] Our group has been particularly interested in the role of HDAC2 in psychiatric and neurodegenerative disorders,[7] and the selective inhibition of this isoform has emerged as a potential epigenetic-based therapeutic approach. Small molecules with improved thermodynamic (IC_{50}, K_i) and/or kinetic (half-life/residence time) selectivity for HDAC1 and 2 will help delineate the respective biological roles of the class I HDACs for complex and chronically treated CNS diseases. Here, we describe our efforts to selectively *tune* the kinetic binding profiles of inhibitors towards HDAC1 and HDAC2, two class I paralogs that share the highest overall amino acid sequence and Zn^{2+} catalytic binding domain similarity

Abbreviations: HATs, histone acetyl transferases; HDACs, histone deacetylases; SAR, structure activity relationship; SKR, structure kinetic relationship; $T_{1/2}$, half-life.

* Corresponding authors. Tel.: +1 617 714 7453 (F.F.W.), +1 857 201 2733 (E.B.H.).
E-mail addresses: fwagner@broadinstitute.org (F.F. Wagner), EHolson@atlasventure.com (E.B. Holson).
† Present address: Atlas Venture, 400 Technology Square, 10th Floor, Cambridge, MA 02139, USA.

http://dx.doi.org/10.1016/j.bmc.2016.06.040
0968-0896/

(86% and 95%, respectively). Binding kinetics represent key and requisite parameters to consider when developing therapeutics[8] to understand and define the target engagement–pharmacodynamic (PD) response relationships. At one extreme, prolonged target engagement (slow-off or pseudo-irreversible inhibitors), as observed for the HDAC1,2 inhibitor compound 60[9] (Supplemental Table S1), may be desirable to affect a prolonged PD response to drive efficacy. Alternatively, prolonged target engagement across multiple HDAC isoforms may drive mechanism-based toxicity, such as thrombocytopenia, and decrease the therapeutic window.[10] By developing a structure–kinetic relationship (SKR)[11] for inhibitors towards HDAC1 and HDAC2, the development of kinetically different binding parameters for each isoform will define optimal target engagement to maximize the PD response and therapeutic index.

2. Material and methods

2.1. Chemistry

See SI for details. Representative procedure for the synthesis of *ortho*-aminoanilide analogs is detailed in Supporting information. All final compounds were confirmed to be of >95% purity based on HPLC LCMS analysis (Alliance 2795, Waters, Milford, MA). Purity was measured by UV absorbance at 210 nm. Identity was determined on a SQ mass spectrometer by positive and negative electrospray ionization. All reagents and solvents were purchased from commercial vendors and used as received. ^{1}H and ^{13}C NMR spectra were recorded on a Bruker 300 MHz or Varian UNITY INOVA 500 MHz spectrometer as indicated. Proton and carbon chemical shifts (δ) are reported in ppm relative to tetramethylsilane (δ 0 for both ^{1}H and ^{13}C) and DMSO-d_6 (^{1}H δ 2.50, ^{13}C δ 39.5). NMR data were collected at 25 °C. Flash chromatography was performed using 40–60 μm Silica Gel (60 Å mesh) on a Teledyne Isco Combiflash Rf system.

2.2. HDAC inhibition assays

All HDACs were purchased from BPS Bioscience. The substrates, Broad Substrate A, and Broad Substrate B, were synthesized in house.[21] All the other reagents were purchased from Sigma. Caliper EZ reader II system was used to collect all data. Purified HDACs were incubated with 2 μM carboxyfluorescein (FAM)-labeled acetylated or trifluoroacetylated peptide substrate (Broad Substrate A and B respectively) and test compound for 60 min at room temperature, in HDAC assay buffer that contained 50 mM HEPES (pH 7.4), 100 mM KCl, 0.01% BSA and 0.001% Tween-20. Reactions were terminated by the addition of the known pan HDAC inhibitor LBH-589 (panobinostat) with a final concentration of 1.5 μM. Substrate and product were separated electrophoretically and fluorescence intensity in the substrate and product peaks was determined and analyzed by Labchip EZ Reader. The reactions were performed in duplicate for each sample. IC_{50} values were automatically calculated by Origion8 using 4 Parameter Logistic Model. The percent inhibition was plotted against the compound concentration, and the IC_{50} value was determined from the logistic dose–response curve fitting by Origin 8.0 software.

2.3. Plasma stability

Plasma stability was determined at 37 °C at 5 h in mouse plasma. Each compound was prepared in duplicate at 5 μM in plasma diluted 50/50 (v/v) with PBS pH 7.4 (0.95% acetonitrile, 0.05% DMSO). Compounds were incubated at 37 °C for 5 h with a 350-rpm orbital shake with time points taken at 0 h and 5 h. Samples were analyzed by UPLC–MS (Waters, Milford, MA) with compounds detected by SIR detection on a single quadrupole mass spectrometer.

2.4. Microsomal stability

Microsomal stability was determined at 37 °C at 60 min in mouse microsomes. Each compound was prepared in duplicate at 1 μM with 0.3 mg/mL microsomes in PBS pH 7.4 (1% DMSO). Compounds were incubated at 37 °C for 60 min with a 350-rpm orbital shake with time points taken at 0 min and 60 min. Samples were analyzed by UPLC–MS (Waters, Milford, MA) with compounds detected by SIR detection on a single quadrupole mass spectrometer.

2.5. Neuronal histone acetylation assays

Measurements of increases in neuronal histone acetylation in mouse fore-brain primary neuronal cultures induced by HDAC inhibitor compounds was performed exactly as described in Fass et al.[12] On the 13th day after generating the cultures, cells were treated for 24 h with compounds at 10 μM. Cells were fixed with formaldehyde, stained with antibodies to acetyl-histone H3, lysine 9 (AcH3K9), or acetyl-histone H4, lysine 12 (AcH4K12), and green fluorescent secondary antibodies, and cellular fluorescence signals were quantitated using laser-scanning cytometry (Acumen eX3, TTP Laptech). To determine the efficacy of HDAC inhibitor compounds, we calculated the percentage of compound-treated cells with a fluorescence signal above a baseline threshold established in vehicle (DMSO) treated cells.

2.6. Protein purification and crystallization

Protein was produced essentially as described in Bressi et al.[13] Briefly, C-terminally His-tagged full-length protein was expressed in insect cells und purified by affinity and size exclusion chromatography. The protein was C-terminally truncated by treatment with trypsin for 1 h at 25 °C. The reaction was stopped by addition of 1 mM PMSF and the protein finally purified by gel filtration chromatography. For crystallization 0.5 μL of the protein solution at 12 mg/ml, containing the ligand at a concentration of 2 mM, was mixed with 0.5 μL of the crystallization buffer (34% PEG400, 0.10 M $NaKPO_4$ pH 6.50, 0.20 M KF). Crystals were harvested in a cryo-loop and frozen directly in liquid nitrogen.

2.7. Data collection, structure solution and refinement

Data collection was performed with synchrotron radiation at the Swiss Light Source, Paul-Scherrer-Institute, Villingen, Switzerland. Crystals belonged to space group $P2_12_12_1$ with cell dimensions a = 92.30 Å, b = 98.01 Å and c = 139.25 Å, $\alpha = \beta = \gamma = 90°$. X-ray intensities and data reduction were evaluated by using the XDS program package[14] (see Table S3 for data collection and processing statistics). Structures were solved and refined with programs of the CCP4 suite (MOLREP and REFMAC5)[15] (see Table S4 for refinement statistics).

3. Results and discussion

We previously reported the discovery of highly ligand efficient carbamide (sp^3-linked) HDAC inhibitors, such as **BRD4884** (Fig. 1), with excellent potency and moderate kinetic selectivity for HDAC2.[16] Following an initial phase (~1 h) of good kinetic selectivity for HDAC1, driven by faster on-rate, **BRD4884** then displays a 7-fold kinetic bias towards HDAC2 versus HDAC1 with residence times of 142 min and 20 min, respectively. In order to obtain a

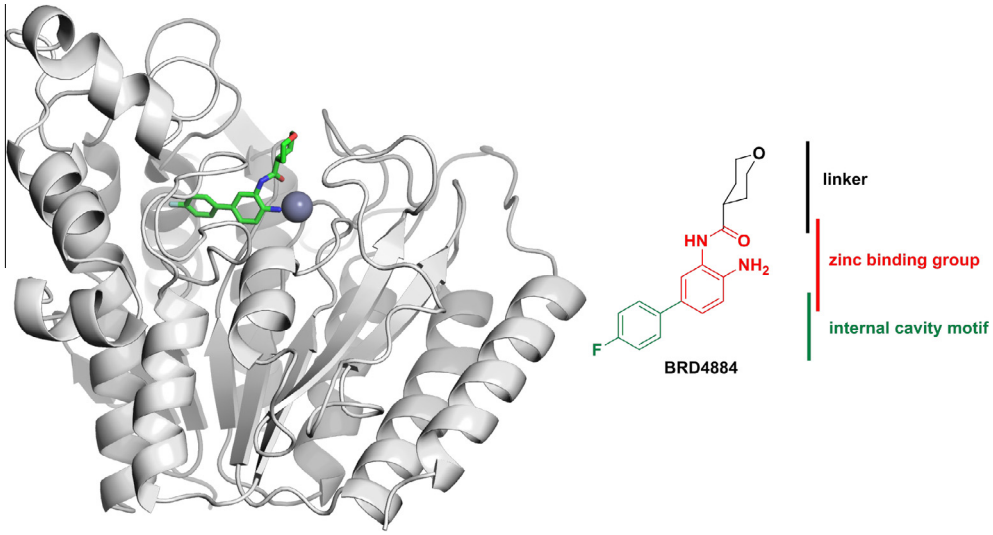

Figure 1. Crystal structure of *h*HDAC2 (ribbon diagram) bound to **BRD4884** (in green) at 1.66 Å resolution; catalytic Zn^{2+} shown in purple; on right: **BRD4884** chemical structure and key binding motifs.

deeper understanding of the structure–activity relationship (SAR) of this novel class of HDAC inhibitors, we report a 1.66 Å resolution structure of human HDAC2 in complex with a carbamide-based *ortho*-aminoanilide, **BRD4884** (Fig. 1).

A C-terminally His-tagged full-length *h*HDAC2 protein was expressed in SF9 insect cells and purified by affinity and size exclusion chromatography. The protein was C-terminally truncated by treatment with trypsin according to Bressi et al.[13] As previously described,[13] the overall protein structure is characterized by a single α/β domain that includes eight β sheets sandwiched between 13 α helices. The active site is characterized by a lipophilic channel of approximately 11 Å that leads from the protein surface to the active site Zn^{2+} ion (Fig. 2A and B) and is lined by Gly154, Phe155, Phe210 and the Zn^{2+} chelating His183. The active site is characterized by a complex coordination sphere between the zinc atom and several key amino acids including Asp181 and His183 (Fig. 2B). Further from the zinc binding site, a hydrophobic 14 Å cavity (the so-called 'foot pocket'[13]) extends towards the core of the protein and is defined by several additional residues including Met35, Phe114, and Leu144 (Fig. 2A and C).

Similar to other small-molecule HDAC inhibitors like SAHA[17] or substituted *N*-(2-aminophenyl)benzamides,[13] **BRD4884** coordinates to the Zn^{2+} ion via the free aniline $-NH_2$, completing its tetrahedral coordination sphere in addition to the side chains of Asp181, His183, and Asp269 with the anilide carbonyl oxygen situated at a distance of 2.8 Å to the Zn^{2+} ion (Fig. 2B). The anilide –NH of **BRD4884** forms an H-bond to the backbone carbonyl oxygen of Gly154. The 11 Å lipophilic channel harbors the tetrahydropyran moiety of **BRD4884** making Van Der Waals contacts with the channel wall. The tetrahydropyran ring adopts a preferential chair conformation allowing the pyran oxygen atom to form a hydrogen bond (3.5 Å) with a conserved water[13,17] at the surface of HDAC2 (Fig. 2B). This ordered water acts as a molecular bridge between the ligand and the protein forming a hydrogen bond with His183 (2.8 Å). Finally, the hydrophobic 14 Å cavity harbors various water molecules that provide a partially hydrophilic environment. These waters could either be displaced or utilized through specific hydrogen bond interactions to achieve greater potency and/or better physicochemical properties. The phenyl ring of **BRD4884** is sandwiched between Leu144 and Met35 and the *para*-fluorine atom points towards Phe114 within the 14 Å cavity.

Informed by this crystal structure and in an effort to further understand and potentially modulate the kinetic binding parameters for HDAC1 or HDAC2, we extended the structure–activity relationship (SAR) at two key portions of the molecule: the internal 14 Å cavity motif (R^2), a 4-fluorophenyl in **BRD4884** and the linker portion (R^1), a 4-tetrahydropyran moiety in **BRD4884** (Fig. 1); then obtained binding kinetics for lead compounds. Modifications of the chelating *ortho*-aminoanilide moiety (aniline and anilide) led to a significant loss in potency (unpublished results), therefore the Zn^{2+}-chelating functional groups were retained throughout this SAR exploration.

First, we explored the space available in the 14 Å cavity (Fig. 2A and C) to understand effects on activity, isoform selectivity and physicochemical properties. As shown in the crystal structure (Fig. 2C), the *para*-fluorophenyl moiety tightly occupies the 14 Å internal cavity. Two water molecules fill an additional small pocket at the back of the 14 Å cavity, presumably, creating a slightly hydrophilic environment that could tolerate less hydrophobic substituents. This small crevice could also accept a functional group with the correct vector off the phenyl ring. The unsubstituted phenyl ring, in compound **1** (Table 1), led to a 5-fold loss in potency towards HDAC2 compared to the *para* fluoro phenyl ring in **BRD4884**. In addition to the increased potency from the *para* fluoro in **BRD4884**, it also conferred increased microsomal stability (54% vs 2% of the parent compound remaining after 2 h in mouse liver microsomes, See Supporting info).

Exploring more hydrophilic substituents within the 14 Å internal cavity, the 4-pyridyl (compound **2**) or 3-pyridyl (compound **3**) substituents led to a significant loss of potency on HDAC1, 2 and 3 (>10-fold loss) consistent with the lipophilic nature of this domain. This observation is unique to the carbamide series as the same 4-pyridyl substituent was optimal in a previously reported constrained urea series.[16] We hypothesize that the divergent SAR between linker and 14 Å internal cavity chemotypes is indicative of ligand defined secondary structural effects which are propagated throughout the catalytic binding domain. Decreased sp^3 steric requirements within the 11 Å channel, minimized in the *constrained* ureas series versus the carbamide series, are able to accommodate more diverse 14 Å internal cavity motifs.

The regiochemistry of the fluoro substituted phenyl ring was also critical. Figure 2C shows that the *p*-fluorophenyl ring fits

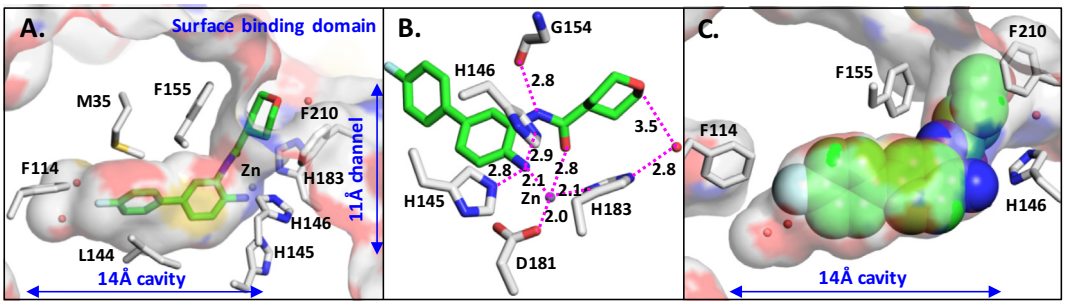

Figure 2. (A) **BRD4884** (green) bound to *h*-HDAC2; (B) ligand (green)–Zn^{2+} (purple) coordination sphere with key interacting amino acids; (C) view of the 14 Å cavity: **BRD4884**, represented as spheres, tightly fits the hydrophobic 14 Å cavity.

Table 1
Mapping the foot pocket: structure activity relationship in the 14 Å internal cavity

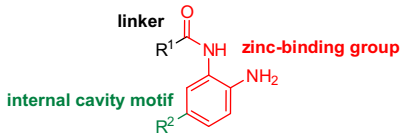

Compound	R^1 group	R^2 group	HDAC isoform inhibition IC_{50}[a] (μM)		
			HDAC1	HDAC2	HDAC3
BRD4884		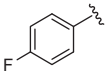	0.029 ± 0.012	0.062 ± 0.031	1.09 ± 0.38
			Residence time $T_{1/2}$ (min)		
			20	143	257
1			0.119 ± 0.057	0.312 ± 0.087	3.85 ± 0.48
2			2.35 ± 0.336	1.42 ± 0.443	>33.33
3			6.45 ± 1.00	7.32 ± 1.04	20.8 ± 1.51
4		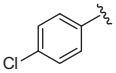	1.52 ± 0.092	2.53 ± 0.661	14.2 ± 1.78
5		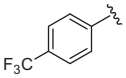	26.7 ± 2.31	>33.33	>33.33
6		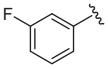	9.67 ± 1.27	12.3 ± 5.07	>33.33

[a] Values are the mean of a minimum of three experiments. Data are shown as IC_{50} values in μM ± standard deviation. Compounds were tested in duplicate in a 12-point dose curve with 3-fold serial dilution starting from 33.3 μM.

tightly in the 14 Å cavity, larger substitutions at the *ortho* or *para* positions were predicted to be disfavored, presumably due to negative Van der Waals interactions with Phe114 (Fig. 2C), and require significant spatial shifts in ligand binding that would destabilize the complex network of hydrogen bond interactions with the zinc atom. Indeed, larger groups at the 4-position of the phenyl ring were not tolerated as both the 4-chlorophenyl (compound **4**) and 4-trifluoromethylphenyl (compound **5**) analogs were weak binders of HDAC1, 2 and 3. However, a substitution at the *meta* position might afford the proper vector to access the additional pockets in distal regions of the 14 Å cavity. Unfortunately, the 3-fluoro substituted compound (**6**) displayed weak activity on HDAC1, 2 and 3 (⩾9 μM on HDAC1, 2 and 3). Other significant changes to these 14 Å occupying motifs (e.g., heteroaryl, cinnamyl, cycloalkenyl) did not yield improvements in potency (data not shown). In summary, the SAR within the 14 Å cavity proved very sensitive and intolerant to changes in substituent size, regiochemistry and hydrophobicity. Since the 4-fluorophenyl group demonstrated optimal binding properties in the internal cavity, it was maintained constant while exploring the SAR of the linker portion of the molecule.

Examination of the **BRD4884**:HDAC2 crystal structure revealed an H-bonded bridging water molecule between the pyran oxygen of **BRD4884** and His183 of HDAC2 (Fig. 2B). In order to evaluate the energetic contribution of this hydrogen bond,[18] the regioisomeric 2-pyran (compounds **7** and **8**) and 3-pyran (**9**) analogs were synthesized and their respective enantiomers separated and tested (Table 2).

In each case, a 20 to 75-fold loss of potency for HDAC2 was observed along with a significant decrease in mouse *plasma* stability indicating an inherent metabolic liability within this series (0% parent remaining after 1 h). The significant loss of activity can be attributed to the loss of the H-bond interaction with the conserved bridging water at the surface of HDAC2 (Fig. 2B) as well as negative interaction between the hydrophilic oxygen atoms pointing towards the lipophilic amino acids of the 11 Å channel (Gly154, Phe155, Phe210 and Leu276). In order to capitalize on potential π–π interactions with the phenylalanines lining the 11 Å channel

Table 2
Structure activity relationship in 11 Å catalytic channel: IC_{50}s for HDAC1, 2 and 3; mouse plasma (after 5 h) and mouse liver microsomes (after 1 h) stability

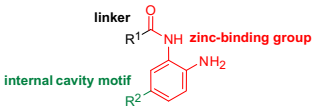

Compound	R^1 group	R^2 group	HDAC isoform inhibition IC_{50}[a] (μM)			Mouse plasma stability % remaining	Mouse liver microsomes stability % remaining
			HDAC1	HDAC2	HDAC3		
BRD4884		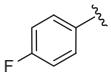	0.029 ± 0.012	0.062 ± 0.031	1.09 ± 0.38	93	54
7		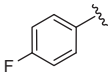	0.467 ± 0.203	1.29 ± 0.399	5.73 ± 1.85	0	nd
8		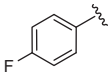	1.43 ± 0.210	1.45 ± 0.486	5.95 ± 0.518	0	nd
9		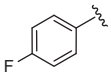	1.22 ± 0.479	4.73 ± 0.299	19.8 ± 7.96	nd	nd
10	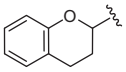	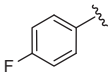	5.59 ± 2.26	6.56 ± 2.66	6.26 ± 3.59	3.7	nd
11	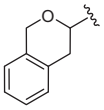	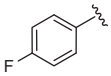	0.045 ± 0.007	0.119 ± 0.050	25.9 ± 7.12	11.1	nd
12	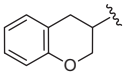	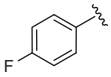	0.072 ± 0.013	0.156 ± 0.071	>33.33	100.3	25
13		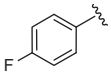	0.123 ± 0.022	0.219 ± 0.001	1.49 ± 0.02	94.1	60
BRD7232		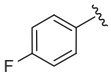	0.192 ± 0.045	0.168 ± 0.052	2.28 ± 0.61	114.5	62
14		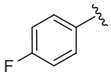	1.45 ± 0.424	1.59 ± 0.372	13.7 ± 0.902	nd	nd

nd = not determined.
[a] Values are the mean of a minimum of three experiments. Data are shown as IC_{50} values in μM ± standard deviation. Compounds were tested in duplicate in a 12-point dose curve with 3-fold serial dilution starting from 33.33 μM.

(Phe155 and Phe210 in HDAC2, Supplemental Fig. S1), a series of benzopyran analogs were synthesized (compounds **10**–**12**). In the 2-benzopyran series, the activity of compound **11** for HDAC2 was improved by a factor of 10 (0.119 μM), however its plasma stability remained mediocre at best (11% remaining after 1 h). In the 3-benzopyran series, the activity of compound **12** for HDAC2 was improved by a factor of 4 (0.156 μM), its plasma stability was also improved (100% remaining after 1 h), however, compound **12** still suffered from poor mouse liver microsomal stability (25% remaining after 2 h). Next, to explore conformational effects of the pyran system, constrained bridged systems were targeted to lock the pyran in the active 'chair' conformation based on the ligand bound structure observed for **BRD4884**, i.e., reinforcing the pyran-O–H-bond with the conserved bridging water (Fig. 2B). Different constrained cyclic systems were synthesized to probe the optimal steric requirements and tolerability within the 11 Å channel. The cyclopropyl fused tetrahydrofuran ([3.1.0] bridged system) in compound **13** and the [3.2.1] bridged system in **BRD7232** afforded good activity (Supplemental Table S2 for IC_{50}s across HDAC1–9) and metabolic stability. The relative stereochemistry in **BRD7232** was important as the bridged diastereomer, compound **14**, was weakly active (Table 2). The absolute stereochemistry of **BRD7232** was determined by X-ray crystallography (Supplemental Fig. S2). The solid-state crystal structure unequivocally demonstrated a *syn* stereochemistry as represented in **BRD7232**.

In order to rationalize the effect of the bridged system in **BRD7232** on binding kinetics, the structure of *h*HDAC2 bound with **BRD7232** was obtained with a 1.72 Å resolution (Fig. 3A and B). The oxabicyclo-octane moiety of **BRD7232** is located in the lipophilic channel lined by Phe210, Phe155, Leu276 and the Zn^{2+} chelating His183. As shown in the space-filling representation in Figure 3B, **BRD7232** optimally fills and occludes the 11 Å channel making Van Der Waals contacts with the channel wall and rim. While the majority of backbone and side chains orientations between the carbamide crystals structures were similar, we did observe a ~1.0 Å shift in Phe155 presumably to accommodate the bridged bicycle. As predicted, the pyran ring of the oxabicyclo-octane moiety was locked into an energetically favored, 'active' chair-like conformation which allowed the pyran oxygen atom to form a hydrogen bond with the bridging water molecule that was also observed in the **BRD4884**:HDAC crystal structure (Fig. 1A).

In order to further characterize the effect of these constrained systems on binding, the kinetic binding parameters were determined for compound **13** and **BRD7232** (Table 3).

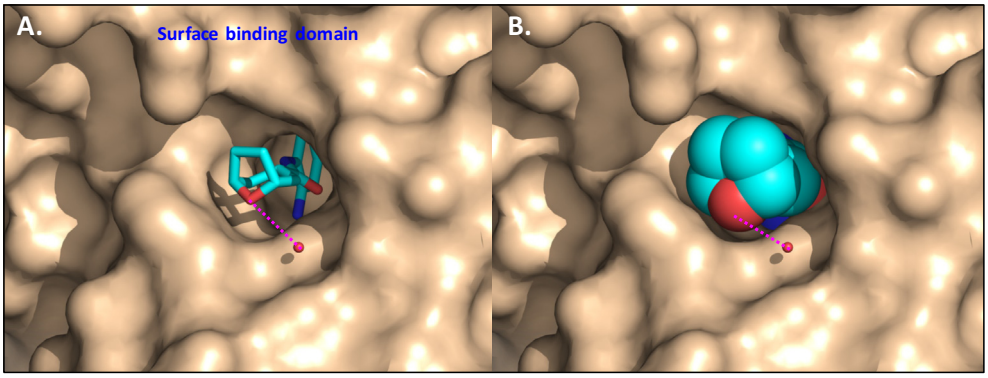

Figure 3. (A) Top view of the X-ray crystal structure of **BRD7232** bound to *h*-HDAC2 superimposed with a solvent accessible surface. The hydrogen bond to the conserved water is maintained; (B) same view with **BRD7232** in space-filling representations.

Table 3
Kinetic parameters for **BRD4884** and **BRD7232**

Kinetic parameters summary		HDAC1				HDAC2				HDAC3			
		K_{on} (min^{-1} μM^{-1})	K_{off} (min^{-1})	$T_{1/2}$ (min)	K_i (μM)	K_{on} (min^{-1} μM^{-1})	K_{off} (min^{-1})	$T_{1/2}$ (min)	K_i (μM)	K_{on} (min^{-1} μM^{-1})	K_{off} (min^{-1})	$T_{1/2}$ (min)	K_i (μM)
BRD4884	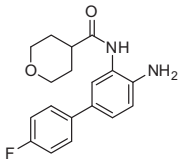	**0.41**	**0.0345**	20	0.084	**0.014**	**0.0049**	143	0.346	0.0013	0.0027	257	2.08
13	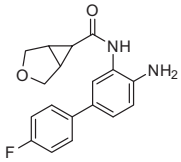	**0.17**	**0.053**	13	0.312	**0.017**	**0.012**	58	0.706	0.0003	0.0032	217	10.7
BRD7232	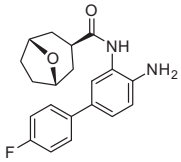	**1.23**	**0.217**	3	0.176	**0.036**	**0.019**	37	0.519	0.00061	0.0053	132	8.68

Bold numbers are meant for emphasis and these numbers are discussed in the text.

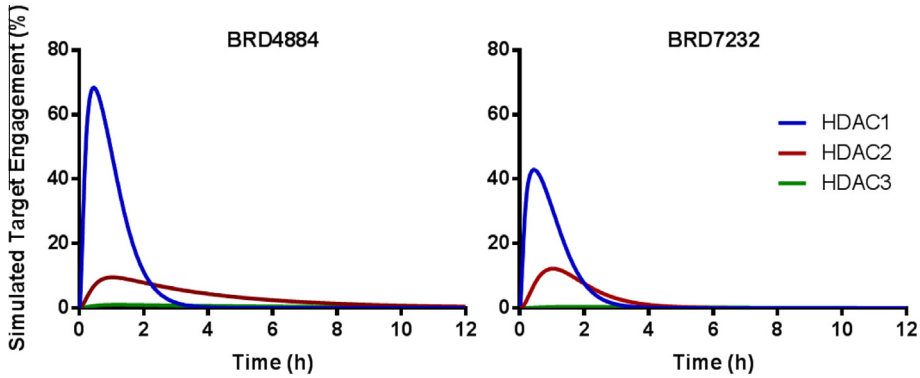

Figure 4. Simulated target engagement profiles for HDAC1, 2 and 3 in mouse brain for **BRD4884** and **BRD7232** with 10 mg/kg intra-peritoneal dose.

Analysis of compound **13** kinetic parameters compared to **BRD4884** revealed a slow-on/*faster*-off kinetics for HDAC2, and *slower*-on/fast-off kinetics for HDAC1. Combined, these changes led to a significant decrease in residence time on HDAC2 ($T_{1/2}$ = 58 min for **13** vs 143 min for **BRD4884**). Analysis of **BRD7232** kinetic parameters (Table 3) revealed a slow-on/*faster*-off kinetics for HDAC2, and *faster*-on/fast-off kinetics for HDAC1, leading to an 12-fold longer residence time on HDAC2 ($T_{1/2}$

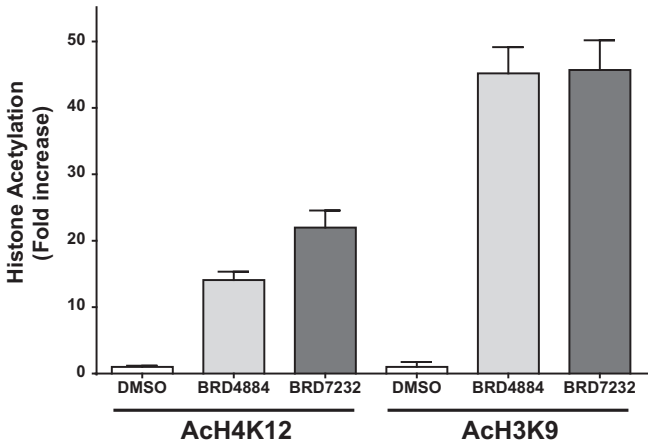

Figure 5. Acetylation status of H3K9 and H4K12 in mouse forebrain primary neuronal cultures cells following 24 h treatment with **BRD4884** and **BRD7232**.

37 min) than on HDAC1 ($T_{1/2}$ 3 min; Table 3). Both compounds demonstrated good selectivity relative to HDAC3 with minimal affinity towards this isoform. When comparing **BRD7232** to **BRD4884**'s kinetic parameters, we observed that for HDAC1, both the on-rate (k_{on}) and off-rate (k_{off}) are faster (3 to 6-fold) leading to a significant decrease in residence time (less engagement) on HDAC1. In comparison, for HDAC2, the on-rate was similarly faster (3-fold), but the shift of the off-rate was not as significant (4-fold) from **BRD4884** to **BRD7232**.

To understand the impact of the kinetic binding parameters in an in vivo setting, the target engagement profiles for HDAC1, 2 and 3 in brain were simulated by numerical integration of differential equations describing the enzyme states.[19] Combining the in vitro kinetic binding parameters, the in vivo pharmacokinetic properties (including brain free fraction, Supplemental Fig. S3) for each compound at equivalent doses (10 mg/kg ip, see Supplemental Fig. 1) and the HDAC enzyme concentration in brain[20] (see Supporting information for detailed description of method and input parameters), a model of target engagement versus time was developed (Fig. 4). The system was assumed to be in rapid equilibrium, while the inhibition complex was driven by the rate constants k_{on} and k_{off}. Total enzyme concentration was fixed over the course of all simulations and the intracellular enzyme concentration was estimated for each isoform according to Wagner et al.[7c] ([HDAC1] = 0.57 μM, [HDAC2] = 0.74 μM, [HDAC3] = 2.0 μM). Good correlation between in vitro and in vivo derived kinetic binding parameters for HDACs 1, 2 and 3 has been demonstrated using brain tissue autoradiography.[20] As described in a previous report,[16] this simulation helps define HDAC isoform selectivity in the dynamic in vivo context.

The overall target engagement and exposure profile of **BRD7232** on HDAC1 (42%, AUC = 56 h^{-1}) compared to **BRD4884** (68%, AUC = 86 h^{-1}) has been significantly reduced, from a peak of 67% engagement to 41%, due to a much faster k_{off} (6 times faster). While the magnitude of target engagement of HDAC2 is very similar between the two compounds (10–12%), the overall duration of target engagement has also been significantly reduced (AUC of 42 vs 25 h^{-1}). **BRD7232** engagement is limited to <3 h on all isoforms. Both compounds exhibit high kinetic selectivity against HDAC3 throughout the simulation. While both **BRD4884** and **BRD7232** demonstrate kinetic selectivity for HDAC1 versus HDAC2, **BRD7232**'s engagement of HDAC1 was significantly reduced, as the engagement of HDAC2 remained similar to **BRD4884**. This demonstrates that the binding kinetics of HDAC inhibitors can be tuned to generate inhibitory compounds with varied target engagement in terms of both magnitude and duration.

Finally, we further validated the functional activity of **BRD7232** toward endogenous HDAC complexes in a cell-based assay by measuring H3K9 and H4K12 acetylation changes in primary mouse neuronal culture. These two histone loci, while not selectively deacetylated by HDAC1 and 2,[8,12] are nevertheless indicative of HDAC1,2 engagement and associated with active transcription. Briefly, mouse forebrain primary neuronal cultures were treated with compounds at 10 μM for 24 h prior to measuring the acetylation status of H3K9 and H4K12 compared to vehicle treatment (Fig. 5). Treatment with **BRD4884** or **BRD7232** displayed significant increases in AcH4K12 and AcH3K9 confirming HDAC1, 2 inhibition in a relevant cell based context.

4. Conclusions

Following our initial report of kinetically selective HDAC2 inhibitors, we now demonstrate that inhibitor binding kinetics for HDACs 1 and 2 can also be tuned by modifying substituents occupying the 11 Å channel. The X-ray crystal structure of human HDAC2 in complex with **BRD4884** and **BRD7232** were solved with excellent resolution and represent the first protein bound crystal structures of non-benzamide *ortho*-aminoanilides. Additionally, we demonstrate that these inhibitors display cell based functional activity through significant increases in AcH4K12 and AcH3K9 in primary neuronal cultures. These novel small molecule inhibitors, which are characterized by different target engagement and binding kinetic profiles on HDAC1 and HDAC2, can be used as tools for probing the biological functions and relevance of the different class I HDAC isoforms. In particular, these compounds enable a refinement of the required inhibitor target engagement (level and duration) to affect the desired pharmacodynamic (PD) response while mitigating other known on-target toxicities, such as thrombocytopenia, that have been linked to the concomitant inhibition of HDAC1 and HDAC2.[10] Additional studies are needed to further enhance the binding kinetics towards one or the other of these highly homologous paralogs. We demonstrate that while a kinetically selective HDAC1 inhibitor with high target engagement is obtainable, a selective HDAC2 inhibitor with a similar binding kinetics profile remains elusive. Additionally, experimental efforts are underway to confirm these target engagement profiles in vivo. The functional translation of these and other selective inhibitors with higher order HDAC complexes, different cell types and tissues, and their role in histone and non-histone acetylation as well as gene expression, remain a field of continued research. Ultimately, our studies open the way for the design of highly optimized selective small molecule HDAC inhibitors relying on structure–*kinetic* in addition to structure–*activity* relationships.

Author contributions

The manuscript was written through contributions of all authors. All authors have given approval to the final version of the manuscript.

Funding sources

This work was supported by the Stanley Medical Research Institute and the NIH/NIDA (S.J.H., R01DA028301).

Acknowledgment

We would like to thank Dr. Steve Johnston for analytical/purification support.

Supplementary data

Spectroscopic characterization of the compounds in this paper; details related to biochemical and cellular studies; details related to simulated target engagement. This material is available free of charge via the Internet at http://pubs.acs.org. hHDAC2 WITH LIGAND **BRD4884**: PDB-Code 5IWG, hHDAC2 WITH LIGAND **BRD7232**: PDB-Code 5IX0.

Supplementary data associated with this article can be found, in the online version, at http://dx.doi.org/10.1016/j.bmc.2016.06.040.

References and notes

1. (a) de Ruijter, A. J.; van Gennip, A. H.; Caron, H. N.; Kemp, S.; van Kuilenburg, A. B. *Biochem. J.* **2003**, *370*, 737; (b) Glaser, K. B.; Staver, M. J.; Waring, J. F.; Stender, J.; Ulrich, R. G.; Davidsen, S. K. *Mol. Cancer Ther.* **2003**, *2*, 151; (c) Marks, P. A.; Richon, V. M.; Miller, T.; Kelly, W. K. *Adv. Cancer Res.* **2004**, *91*, 137; (d) Spange, S.; Wagner, T.; Heinzel, T.; Kramer, O. H. *Int. J. Biochem. Cell Biol.* **2009**, *41*, 185.
2. Khan, O.; La Thangue, N. B. *Immunol. Cell Biol.* **2012**, *90*, 85.
3. (a) Chou, D. H.; Holson, E. B.; Wagner, F. F.; Tang, A. J.; Maglathlin, R. L.; Lewis, T. A.; Schreiber, S. L.; Wagner, B. K. *Chem. Biol.* **2012**, *19*, 669; (b) Feng, D.; Liu, T.; Sun, Z.; Bugge, A.; Mullican, S. E.; Alenghat, T.; Liu, X. S.; Lazar, M. A. *Science* **2011**, *331*, 1315.
4. (a) Andrews, K. T.; Haque, A.; Jones, M. K. *Immunol. Cell Biol.* **2012**, *90*, 66; (b) Barton, K. M.; Archin, N. M.; Keedy, K. S.; Espeseth, A. S.; Zhang, Y. L.; Gale, J.; Wagner, F. F.; Holson, E. B.; Margolis, D. M. *PLoS ONE* **2014**, *9*, e102684; (c) Rotili, D.; Simonetti, G.; Savarino, A.; Palamara, A. T.; Migliaccio, A. R.; Mai, A. *Curr. Top. Med. Chem.* **2009**, *9*, 272.
5. (a) Graff, J.; Rei, D.; Guan, J. S.; Wang, W. Y.; Seo, J.; Hennig, K. M.; Nieland, T. J.; Fass, D. M.; Kao, P. F.; Kahn, M.; Su, S. C.; Samiei, A.; Joseph, N.; Haggarty, S. J.; Delalle, I.; Tsai, L. H. *Nature* **2012**, *483*, 222; (b) Graff, J.; Tsai, L. H. *Annu. Rev. Pharmacol. Toxicol.* **2013**, *53*, 311; (c) Nestler, E. J. *Biol. Psychiatry* **2009**, *65*, 189; (d) Weiwer, M.; Lewis, M. C.; Wagner, F. F.; Holson, E. B. *Future Med. Chem.* **2013**, *5*, 1491.
6. Wagner, F. F.; M, W.; Lewis, M. C.; Holson, E. B. *Neurotherapeutics* **2013**, *10*, 589.
7. (a) Guan, J. S.; Haggarty, S. J.; Giacometti, E.; Dannenberg, J. H.; Joseph, N.; Gao, J.; Nieland, T. J.; Zhou, Y.; Wang, X.; Mazitschek, R.; Bradner, J. E.; DePinho, R. A.; Jaenisch, R.; Tsai, L. H. *Nature* **2009**, *459*, 55; (b) Schroeder, F. A.; Lewis, M. C.; Fass, D. M.; Wagner, F. F.; Zhang, Y. L.; Hennig, K. M.; Gale, J.; Zhao, W. N.; Reis, S.; Barker, D. D.; Berry-Scott, E.; Kim, S. W.; Clore, E. L.; Hooker, J. M.; Holson, E. B.; Haggarty, S. J.; Petryshen, T. L. *PLoS ONE* **2013**, *8*, e71323; (c) Wagner, F. F.; Zhang, Y. L.; Fass, D. M.; Joseph, N.; Gale, J. P.; Weiwer, M.; McCarren, P.; Fisher, S. L.; Kaya, T.; Zhao, W. N.; Reis, S. A.; Hennig, K. M.; Thomas, M.; Lemercier, B. C.; Lewis, M. C.; Guan, J. S.; Moyer, M. P.; Scolnick, E.; Haggarty, S. J.; Tsai, L. H.; Holson, E. B. *Chem. Sci.* **2015**, *6*, 804.
8. Naldi, M.; Calonghi, N.; Masotti, L.; Parolin, C.; Valente, S.; Mai, A.; Andrisano, V. *Proteomics* **2009**, *9*, 5437.
9. (a) Methot, J. L.; Chakravarty, P. K.; Chenard, M.; Close, J.; Cruz, J. C.; Dahlberg, W. K.; Fleming, J.; Hamblett, C. L.; Hamill, J. E.; Harrington, P.; Harsch, A.; Heidebrecht, R.; Hughes, B.; Jung, J.; Kenific, C. M.; Kral, A. M.; Meinke, P. T.; Middleton, R. E.; Ozerova, N.; Sloman, D. L.; Stanton, M. G.; Szewczak, A. A.; Tyagarajan, S.; Witter, D. J.; Secrist, J. P.; Miller, T. A. *Bioorg. Med. Chem. Lett.* **2008**, *18*, 973; (b) Moradei, O. M.; Mallais, T. C.; Frechette, S.; Paquin, I.; Tessier, P. E.; Leit, S. M.; Fournel, M.; Bonfils, C.; Trachy-Bourget, M. C.; Liu, J.; Yan, T. P.; Lu, A. H.; Rahil, J.; Wang, J.; Lefebvre, S.; Li, Z.; Vaisburg, A. F.; Besterman, J. M. *J. Med. Chem.* **2007**, *50*, 5543.
10. Wilting, R. H.; Yanover, E.; Heideman, M. R.; Jacobs, H.; Horner, J.; van der Torre, J.; DePinho, R. A.; Dannenberg, J. H. *EMBO J.* **2010**, *29*, 2586.
11. Vilums, M.; Zweemer, A. J.; Yu, Z.; de Vries, H.; Hillger, J. M.; Wapenaar, H.; Bollen, I. A.; Barmare, F.; Gross, R.; Clemens, J.; Krenitsky, P.; Brussee, J.; Stamos, D.; Saunders, J.; Heitman, L. H.; Ijzerman, A. P. *J. Med. Chem.* **2013**, *56*, 7706.
12. Fass, D. M.; Reis, S. A.; Ghosh, B.; Hennig, K. M.; Joseph, N. F.; Zhao, W. N.; Nieland, T. J.; Guan, J. S.; Kuhnle, C. E.; Tang, W.; Barker, D. D.; Mazitschek, R.; Schreiber, S. L.; Tsai, L. H.; Haggarty, S. J. *Neuropharmacology* **2013**, *64*, 81.
13. Bressi, J. C.; Jennings, A. J.; Skene, R.; Wu, Y.; Melkus, R.; De Jong, R.; O'Connell, S.; Grimshaw, C. E.; Navre, M.; Gangloff, A. R. *Bioorg. Med. Chem. Lett.* **2010**, *20*, 3142.
14. Kabsch, W. *J. Appl. Crystallogr.* **1993**, *26*, 795.
15. Winn, M. D.; Ballard, C. C.; Cowtan, K. D.; Dodson, E. J.; Emsley, P.; Evans, P. R.; Keegan, R. M.; Krissinel, E. B.; Leslie, A. G.; McCoy, A.; McNicholas, S. J.; Murshudov, G. N.; Pannu, N. S.; Potterton, E. A.; Powell, H. R.; Read, R. J.; Vagin, A.; Wilson, K. S. *Acta Crystallogr. D Biol. Crystallogr.* **2011**, *67*, 235.
16. Wagner Florence, F.; Zhang, Y.-L.; Fass, D. M.; Joseph, N.; Gale, J. P.; Weiwer, M.; McCarren, P.; Fisher, S. L.; Kaya, T.; Zhao, W.-N.; Reis, S. A.; Hennig, K. M.; Thomas, M.; Lemercier Berenice, C.; Lewis, M. C.; Guan, J.-S.; Moyer, M. P.; Scolnick, E. M.; Haggarty, S. J.; Tsai, L.-H.; Holson Edward, B. *Chem. Sci.* **2015**, *6*, 804.
17. Lauffer, B. E.; Mintzer, R.; Fong, R.; Mukund, S.; Tam, C.; Zilberleyb, I.; Flicke, B.; Ritscher, A.; Fedorowicz, G.; Vallero, R.; Ortwine, D. F.; Gunzner, J.; Modrusan, Z.; Neumann, L.; Koth, C. M.; Lupardus, P. J.; Kaminker, J. S.; Heise, C. E.; Steiner, P. *J. Biol. Chem.* **2013**, *288*, 26926.
18. Freire, E. *Drug Discovery Today* **2008**, *13*, 869.
19. Walkup, G. K.; You, Z.; Ross, P. L.; Allen, E. K.; Daryaee, F.; Hale, M. R.; O'Donnell, J.; Ehmann, D. E.; Schuck, V. J.; Buurman, E. T.; Choy, A. L.; Hajec, L.; Murphy-Benenato, K.; Marone, V.; Patey, S. A.; Grosser, L. A.; Johnstone, M.; Walker, S. G.; Tonge, P. J.; Fisher, S. L. *Nat. Chem. Biol.* **2015**, *11*, 416.
20. Wang, Y.; Zhang, Y. L.; Hennig, K.; Gale, J. P.; Hong, Y.; Cha, A.; Riley, M.; Wagner, F.; Haggarty, S. J.; Holson, E.; Hooker, J. *Epigenetics* **2013**, *8*, 756.
21. Zhang, Y.-L.; Holson, E.; Wagner, F. F. Fluorescent substrates for determining lysine modifying enzyme activity, 2013, WO 2013067391.